Mesopotamian Journal of Civil Engineering
Vol.2026, **pp**. 114–124
DOI: https://doi.org/10.58496/MJCE/2026/010; ISSN: 3006-1148
https://mesopotamian.press/journals/index.php/MJCE

Research Article

Performance Assessment of Construction Joints in Reinforced Concrete T-Beams

Falah J. Alkhafaji[1], Mohammed A. Jennam[1], Ashraf Hameed Alsalmani[2, *], Amer F. Izzet[3]

[1] *Civil Engineering Department, University of Shatrah, Dhi Qar, Iraq.*

[2] *Office of the Speaker, Iraqi Council of Representatives, Baghdad, Iraq.*

[3] *Civil Engineering Department, College of Engineering, University of Baghdad, Baghdad, Iraq.*

ARTICLE INFO

Article History
Received 19 Jul 2026
Revised 24 Aug 2026
Accepted 28 Sep 2026
Published 02 Nov 2026

Keywords
Construction joint,
Inclined joint,
Keyed joint,
Reinforced concrete,
T-beam; Vertical joint.

ABSTRACT

Six reinforced-concrete T-beams were tested under monotonic three-point bending to compare construction-joint configurations. Each specimen had a 200 mm wide, 50 mm thick flange, a 100 mm wide, 150 mm deep web, an overall length of 1200 mm and an effective span of 1000 mm. One monolithic reference beam was compared with two horizontal-joint specimens and three specimens with vertical, inclined or keyed midspan joints. Measured responses comprised first-visible-crack load, ultimate load and midspan deflection, supplemented by visual crack observations. Relative to the 56 kN reference capacity, the horizontal-joint specimens reached 50 kN, a 10.7% reduction; the keyed specimen reached 55 kN, a 1.8% reduction. At the common 30 kN comparison load, the keyed specimen retained 93.5% of the reference secant stiffness. All three deflection checkpoints exceeded first-visible-crack loads and do not establish uncracked stiffness. With one specimen per configuration and no direct interface-slip or reinforcement-strain measurements, these findings are descriptive comparisons of measured global responses. They do not establish statistical equivalence, isolate force-transfer mechanisms or provide general design rules.

1. INTRODUCTION

Concrete placement is not always completed in a single uninterrupted operation. Equipment failure, interruptions in material supply, and delays in concrete delivery can stop casting, particularly in members that require a relatively large volume of concrete. When placement is resumed after the previously cast concrete has begun to set, an interface is formed between the two placements and the structural member must transfer forces across that interface [1-5].

Such an interface is treated as a construction joint. The structural relevance of a construction joint lies in its ability to preserve force transfer across two concrete placements that were not cast monolithically. In reinforced-concrete beams, this transfer is provided through the combined action of reinforcement crossing the interface and the contact developed between the old and new concrete. The continuous reinforcement maintains flexural continuity and contributes to dowel action, whereas the concrete interface participates in shear transfer [6]. The resulting behavior is therefore influenced not only by the existence of the joint, but also by its position and orientation within the member. Because different joint arrangements intersect the internal stress field differently, joints located in regions of relatively high bending or shear demand may modify cracking and deformation even when the longitudinal reinforcement remains continuous.

Previous experimental studies have demonstrated that the structural effect of a construction joint can vary substantially with specimen type, interface detail, and loading condition. Aziz and Ajeel [7] examined reinforced-concrete T-beams containing flange openings and construction joints and reported an approximately 27% reduction in shear strength for the specimen incorporating a cold joint. Issa et al. [8], using plain-concrete beams with a vertical joint at mid-span, reported reductions in modulus of rupture ranging from 24% to 83%. Vertical construction joints were also investigated by Gerges et al. [9], who examined their influence on the flexural capacity of singly reinforced concrete beams.

The available literature also indicates that interface geometry can modify the response of the jointed member. Jang et al. [10] reported improved shear resistance in UHPC construction joints for the investigated grooved interface treatments. In concrete slabs, Bin Osman et al. [11] found that structural performance varied with the adopted joint configuration; the inclined-joint specimen showed comparatively favorable load and energy-absorption behavior, whereas the Hy-Rib Mesh configuration exhibited the highest reported stiffness among the jointed specimens. Similar trends were reported by Jabir et al. [12] for

*Corresponding author. Email: ashraf.hameed@coagri.uobaghdad.edu.iq

reinforced-concrete beams, where horizontal joints performed more favorably when positioned in the compression zone, while inclined joints produced only a limited reduction in collapse load.

Collectively, these studies show that the behavior of a construction joint is governed by more than the presence of a casting discontinuity. Joint location, orientation, and interface geometry all contribute to the structural response. However, direct comparative evidence covering several joint configurations within a single reinforced-concrete T-beam test program remains limited. This gap is especially relevant for T-sections, where the flange and web provide multiple practical locations for horizontal construction joints.

Accordingly, the present work compares horizontal joints at different levels with vertical, inclined, and keyed joints located at mid-span. The comparison is based on first cracking, ultimate resistance, crack pattern, failure mode, and load-deflection response. The objective is to identify the joint arrangement that causes the least deterioration relative to a monolithically cast reference T-beam.

2. EXPERIMENTAL PROGRAM

Six simply supported reinforced-concrete T-beams were included in the test program. The specimens had the same nominal geometry and reinforcement arrangement. Each beam was 1200 mm long and was tested over an effective span of 1000 mm. The web was 100 mm wide and 150 mm deep, and the flange was 200 mm wide and 50 mm thick. The longitudinal and transverse reinforcement arrangement is shown in Fig. 1. Constant nominal geometry and reinforcement support a descriptive comparison, but the lack of replicate beams prevents separation of configuration effects from specimen variability.

One specimen was cast continuously and designated as the reference beam (RB). The remaining specimens were cast in two stages. Group A contained the horizontal-joint configurations, whereas Group B contained the vertical, inclined, and keyed joints located at mid-span. The specimen designations and joint arrangements are summarized in Table 1 and illustrated in Fig. 2.

The joint type and joint position were therefore the principal experimental variables. No change in beam span, cross-section, or nominal reinforcement arrangement was introduced between the reference and jointed specimens. The horizontal arrangements examine interfaces within the web and at the flange level. The midspan arrangements compare shapes in the region of maximum nominal bending moment. Figure 2 shows a 200 mm longitudinal projection of the inclined interface through the 200 mm overall depth, corresponding to a nominal 45-degree inclination to the beam axis, and 100 mm horizontal and vertical dimensions for the keyed step. These are drawing dimensions, not independent as-built measurements; the tested interface profile was not surveyed.

2.1 Material Properties

The reinforcement properties are listed in Table 2. The concrete was assessed using 150 × 150 × 150 mm cubes, with team-reported 28-day cube strengths listed by casting stage in Table 2a. Cylinder strength was not measured directly. For calculations explicitly requiring a cylinder-equivalent value, an approximate factor of 0.80 was applied to the team-reported mean cube strength. Cement and aggregate testing followed Iraqi Standard Specifications IQS No. 5-2019 and IQS No. 45-1984, respectively. The experimental documentation cites ASTM A615/A615M-16 [13] for reinforcing bars and ASTM A496/A496M-07 [14] for deformed wire. The latter is a historical specification withdrawn in 2013; its citation identifies the reported specification and does not establish compliance with a current edition.

2.1.1 Concrete Cube Results and Estimated Cylinder-Equivalent Strength

Table 2a reproduces the team-reported cube readings for the shared experimental campaign: 29.6, 30.1 and 30.3 MPa for stage 1, and 29.5, 30.0 and 30.4 MPa for stage 2. The respective means are 30.00 and 29.97 MPa, with sample standard deviations of 0.36 and 0.45 MPa. The source is a companion manuscript from the same campaign, currently under review, rather than independently inspected laboratory sheets. Accordingly, these are team-reported material values with limited documentary traceability. Their dispersion describes cube specimens and cannot quantify variation between structural T-beams. No stage-wise 7-day readings are reported here.

For the illustrative cracking calculation only, the assumed conversion is $f'_{c,est} = 0.80\, f_{cu,mean}$, giving 24.00 MPa for stage 1 and 23.97 MPa for stage 2. The factor is an analytical assumption rather than a measured conversion for this mixture. Neither value is a directly measured cylinder strength, and neither establishes equivalence of the two placements. The previously stated 25 MPa value is retained only as an alternative assumption when reproducing the earlier calculation.

According to the experimental-team account, both placements used the same mixture, the inter-pour interval was 48 h, and hardened surfaces were cleaned with a steel wire brush, mechanically roughened and moistened before second placement. Wet curing was reported for seven days. Quantified surface-profile and moisture measurements are unavailable; a saturated-surface-dry condition is not asserted. The monolithic reference had no inter-pour interval.

2.2 Test Setup and Loading Procedure

The experimental-team account specifies monotonic three-point bending with hydraulic load control, a nominal rate of 4 kN/min, and pauses at 5 kN increments to observe cracks and record deflection. Load was monitored with a load cell, and midspan deflection with dial gauges graduated at 0.01 mm per division. The team reports machine calibration by the Iraqi Central Organization for Standardization and Quality Control; certificate details, validity dates, load-cell accuracy and gauge-specific calibration were unavailable. Gauge count and precise attachment were not documented sufficiently for independent reconstruction. Fig. 3 illustrates the nominal support and load arrangement, rather than the complete instrumentation layout. Gauge graduation describes resolution rather than verified accuracy.

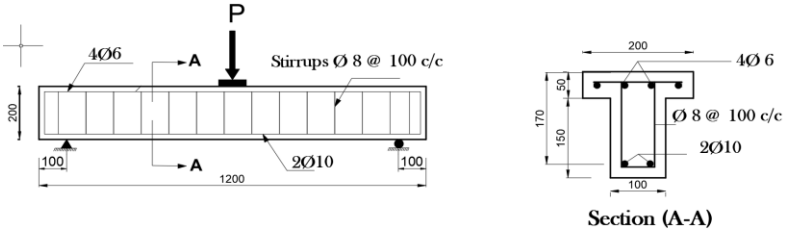
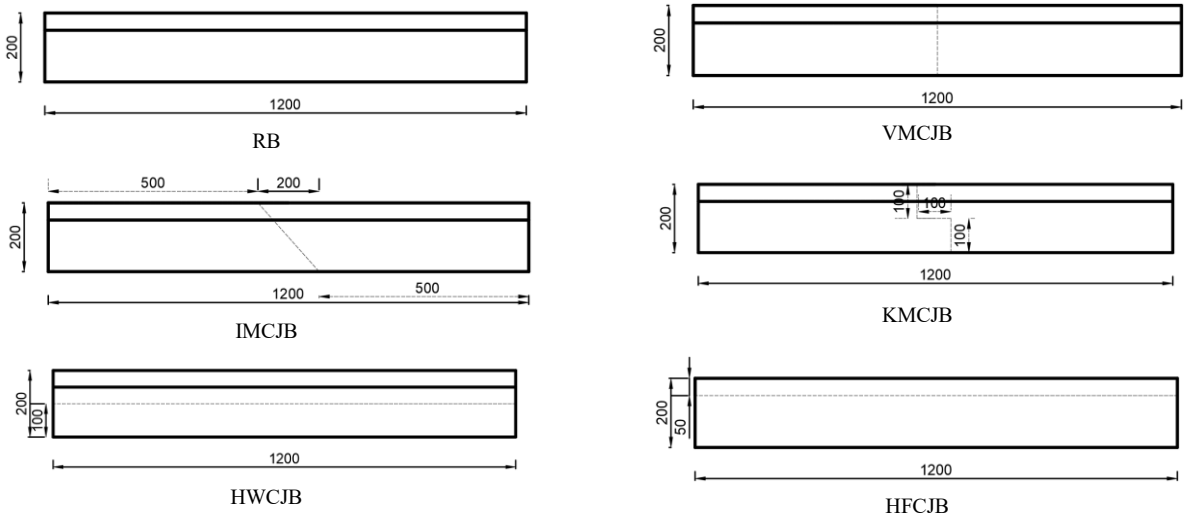


Fig. 1. Typical dimensions and reinforcement details of the T-beams (all dimensions in mm).



Reference (R), beam(B), Vertical (V), mid(M), Construction(C), Joint(J), Inclined (I), key(K), Horizontal(H), web(W), and Flange(F).

Fig. 2. The experimental details of tested beams (all dimensions in mm).

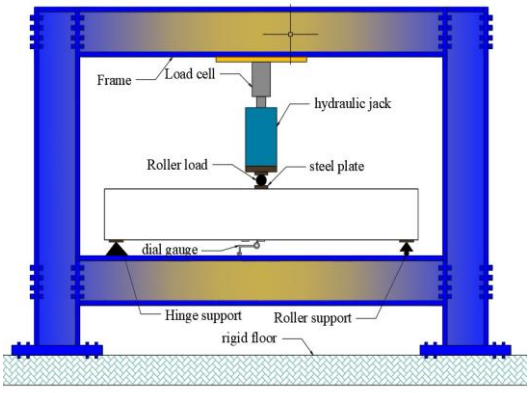


Fig. 3. Illustrative three-point bending frame with hinged and roller supports and a central load point. This schematic does not document the exact dial-gauge installation or calibration.

TABLE I. TEST MATRIX AND CONSTRUCTION-JOINT CONFIGURATIONS. RB IS THE SAME REFERENCE SPECIMEN IN GROUPS A AND B.

Group	Description	Specimens
A	Reference beam	RB
	Horizontal construction joint	HWCJB
		HFCJB
B	Reference beam	RB
	Construction joint at mid-span (vertical, inclined, or keyed)	VMCJB
		IMCJB
		KMCJB

TABLE II. REPORTED MATERIAL PROPERTIES.

Material	Diameter (mm)	Yield strength (MPa)	Estimated 28-day cylinder-equivalent strength, f'c,est (MPa)	Ultimate tensile strength (MPa)	Elastic modulus (GPa)
Concrete	—	—	≈24.0 (not tested as cylinders)	—	—
Reinforcing steel	4	370	—	510	200
	6	430	—	550	200
	10	550	—	630	200

TABLE IIA. TEAM-REPORTED 28-DAY CUBE STRENGTHS BY CASTING STAGE FOR 150 MM CUBES. ORIGINAL SIGNED LABORATORY SHEETS WERE NOT AVAILABLE FOR INDEPENDENT VERIFICATION.

Casting stage	Cube 1 (MPa)	Cube 2 (MPa)	Cube 3 (MPa)	Mean ± sample SD (MPa)
First	29.6	30.1	30.3	30.00 ± 0.36
Second	29.5	30.0	30.4	29.97 ± 0.45

Note to Table 2. The approximately 24 MPa entry is an assumed cylinder-equivalent value calculated from the team-reported approximately 30 MPa cube mean using f'c,est = 0.80 fcu,mean. It is not a cylinder-test result or a validated conversion for this mixture.

The reported procedure identifies the available loading and displacement information. No numerical instrument uncertainty is assigned because accuracy specifications and traceable calibration records were unavailable.

3. EXPERIMENTAL RESULTS AND DISCUSSION

3.1 First Cracking and Ultimate Load

The first visible-crack load was used as an experimental cracking indicator. The conventional theoretical value was recalculated from gross-section elastic theory using the T-beam dimensions and an explicitly stated cylinder-strength assumption. This calculation is a homogeneous-section benchmark, not a validated prediction of jointed-beam interface cracking. The gross-section elastic relation is used as a conventional mechanics baseline [15].

$$f_r = \frac{M_{cr}\, y_t}{I_g} \quad (1)$$

$$P_{cr,th} = \frac{4\, f_r\, I_g}{L\, y_t} \times 10^{-3}\ (kN) \quad (2)$$

Equation (2) assumes a homogeneous gross section and central point loading, with fr in MPa, Ig in mm⁴ and L and yt in mm; 10^{-3} converts N to kN. It does not represent an interface discontinuity. Table 3 gives the reported first-visible-crack and ultimate loads. Visual detection identifies first visible cracking rather than the precise instant of crack initiation.

- **Conventional theoretical cracking calculation**

Using the recorded T-section geometry (flange 200 × 50 mm; web 100 × 150 mm below the flange), the gross area is 25,000 mm². The neutral-axis depth from the top is 85.0 mm, the extreme tension-fiber distance is yt = 115.0 mm, and the gross second moment of area is Ig = 90.208 × 10^6 mm⁴. Assuming fr = 0.62√f'c (MPa), Mcr = fr Ig/yt and Pcr,th = 4Mcr/L for a simply supported beam with a central point load and L = 1000 mm.

For the previously reported f'c = 25 MPa, these equations yield fr = 3.100 MPa, Mcr = 2.432 kN·m and Pcr,th = 9.726 kN (≈9.73 kN); the earlier theoretical value is therefore arithmetically consistent with that assumption. With the assumed cylinder-equivalent strength f'c,est ≈24 MPa, fr = 3.038 MPa, Mcr = 2.383 kN·m and Pcr,th ≈9.53 kN. The reference beam first-visible-crack load of 13.0 kN exceeds these respective benchmarks by 33.7% and approximately 36.4%. Visual crack detection and the assumed modulus-of-rupture relation are possible contributors to the discrepancy, but their contributions have not been separately measured. Because the interface is not represented in the homogeneous model, these estimates must not be interpreted as predictions of each construction-joint specimen.

The ratio Pcr/Pu ranged from 18.0% to 23.2% among the tested beams. The reference specimen reached a first visible crack load of 13 kN and an ultimate load of 56 kN.

The response at first cracking was sensitive to joint configuration. Both horizontal-joint specimens, HWCJB and HFCJB, cracked at 9 kN, corresponding to a 30.8% reduction relative to RB. VMCJB and IMCJB each cracked at 10 kN, a 23.1% reduction. KMCJB reached 12 kN and therefore showed the smallest reduction in first-crack load, 7.7%. These results place the keyed joint closest to the monolithic reference beam at the onset of visible cracking.

A similar ranking was obtained for ultimate resistance. HWCJB and HFCJB failed at 50 kN, which is 10.7% below the 56 kN capacity of RB. The ultimate loads of VMCJB and IMCJB were 52 and 53 kN, representing reductions of 7.1% and 5.4%, respectively. KMCJB reached 55 kN and differed from RB by 1.8% (1.79% before rounding). The better performance of the inclined and keyed configurations is consistent with a larger or mechanically interlocked interface; however, the present tests quantify the global beam response and do not independently measure interface shear transfer.

TABLE III. FIRST-VISIBLE-CRACK AND ULTIMATE LOADS. REPEATED RB ENTRIES REFER TO THE SAME SPECIMEN.

Group	Specimen	First-visible-crack load, Pcr (kN)	Ultimate load, Pu (kN)	Pcr/Pu (%)	Reduction in first-visible-crack load vs. RB (%)	Reduction in ultimate load vs. RB (%)
A	RB	13	56	23.2	0.0	0.0
	HWCJB	9	50	18.0	30.8	10.7
	HFCJB	9	50	18.0	30.8	10.7
B	RB	13	56	23.2	0.0	0.0
	VMCJB	10	52	19.2	23.1	7.1
	IMCJB	10	53	18.9	23.1	5.4
	KMCJB	12	55	21.8	7.7	1.8

3.2 Crack Development and Failure Mode

For all specimens, the first visible flexural cracks formed at the soffit in the vicinity of mid-span, where the positive bending moment is maximum. With increasing load, these cracks widened and propagated upward. Additional flexural cracks developed along the span, and diagonal cracking was observed closer to the supports in the shear-dominated regions.

The observed crack and failure appearances were consistent with flexure-dominated behavior. Reinforcement yielding was not established by strain measurements. No obvious macroscopic interface separation was reported visually; this does not establish zero relative slip or quantify interface opening. Crack widths, spacing and propagation rates were not measured with calibrated instruments and are discussed qualitatively. Figure 4 shows the documented crack patterns. Measured load and deflection differences describe member response without isolating a local interface mechanism.

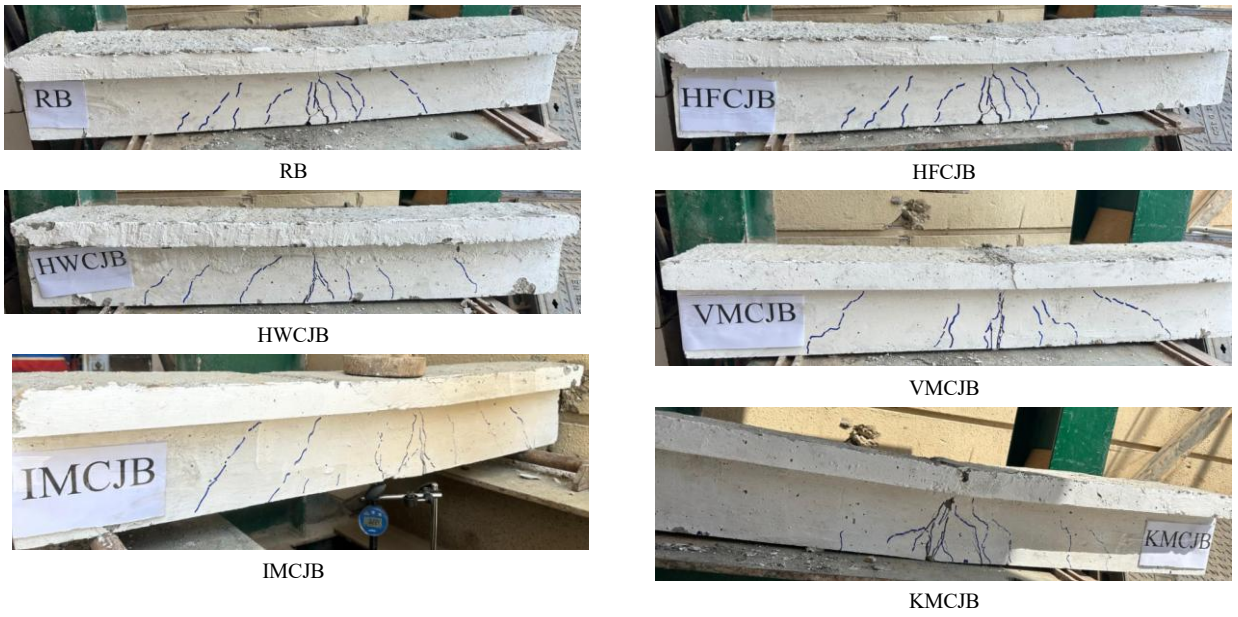


Fig. 4. Crack patterns of the tested reinforced-concrete T-beams.

3.3 Load-Deflection Response

Figures 5 and 6 show the original experimental load-deflection curves. Table 4 compares the existing numerical midspan-deflection checkpoints at 15, 30 and 50 kN. The authors confirmed the specimen identification in the original curves; the HWCJB and HFCJB checkpoint assignments have therefore been corrected to follow those curves. No additional numerical readings have been digitized from the images. All three checkpoints exceed the first-visible-crack loads of 9-13 kN. The 30 kN point is a common intermediate comparison load without a code-based service-load calculation, and 50 kN equals the ultimate load of both horizontal-joint specimens. The original curve images preserve the reported response history, but complete raw numerical histories remain unavailable for independent reconstruction or reliable tangent-stiffness estimation. For Group A, HWCJB showed deflection increases of 31.82%, 37.21% and 29% at 15, 30 and 50 kN, respectively, relative to RB. The corresponding increases for HFCJB were 45.45%, 46.51% and 35%. Thus, the horizontal joint at the flange level produced the larger deformation at these three comparison loads. These are descriptive comparisons of the individual specimens; the test program does not separate the contributions of interface slip, cracking and section stiffness.

The same trend was evident in Group B, but the magnitude depended strongly on joint geometry. VMCJB showed the largest increase in deflection: 27.27% at 15 kN, 37.21% at 30 kN, and 27% at 50 kN. IMCJB showed increases of 18.18%, 27.91%, and 20%, respectively. KMCJB remained much closer to the reference beam, with increases of 4.55%, 6.98%, and 5%. The keyed configuration therefore provided the best load-deflection performance among the jointed specimens tested at mid-span.

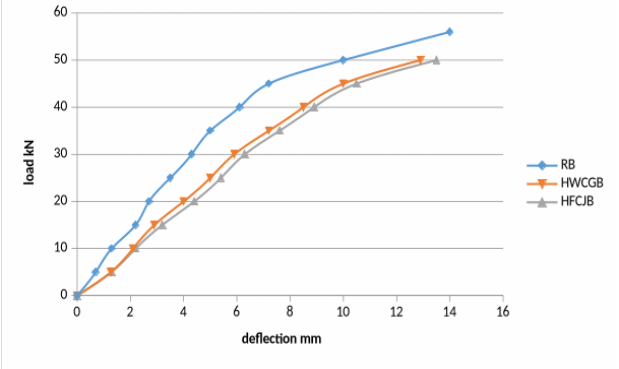


Fig. 5. Load-deflection response of RB, HWCJB and HFCJB. Original experimental curves retained with author-confirmed specimen identification. HWCGB in the original legend denotes HWCJB.

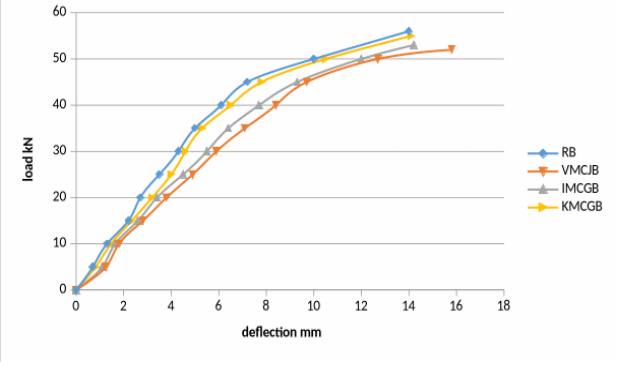


Fig. 6. Load-deflection response of RB, VMCJB, IMCJB and KMCJB. Original experimental curves retained with author-confirmed specimen identification. IMCGB and KMCGB in the original legend denote IMCJB and KMCJB.

TABLE IV. MIDSPAN DEFLECTION AT THE COMMON LOADS AND ULTIMATE LOAD. ΔΔ IS THE PERCENTAGE INCREASE RELATIVE TO RB AT THE SAME LOAD; ΔPU IS THE PERCENTAGE REDUCTION IN ULTIMATE LOAD RELATIVE TO RB. REPEATED RB ENTRIES IDENTIFY THE SAME REFERENCE SPECIMEN.

Group	Specimen	δ15 (mm)	Δδ15 (%)	δ30 (mm)	Δδ30 (%)	δ50 (mm)	Δδ50 (%)	Pu (kN)	ΔPu (%)
A	RB	2.2	0.00	4.3	0.00	10.0	0.00	56	0.00
A	HWCJB	2.9	31.82	5.9	37.21	12.9	29.00	50	10.71
A	HFCJB	3.2	45.45	6.3	46.51	13.5	35.00	50	10.71
B	RB	2.2	0.00	4.3	0.00	10.0	0.00	56	0.00
B	VMCJB	2.8	27.27	5.9	37.21	12.7	27.00	52	7.14
B	IMCJB	2.6	18.18	5.5	27.91	12.0	20.00	53	5.36
B	KMCJB	2.3	4.55	4.6	6.98	10.5	5.00	55	1.79

3.4 Quantitative Secant-Stiffness Assessment

At each common applied load, secant stiffness was calculated as $K_{sec}(P) = P/\delta(P)$. Stiffness retention was evaluated relative to the single monolithic reference beam at the same load, $K_{sec,j}/K_{sec,RB} = \delta_{RB}/\delta_j$. The three comparison loads (15, 30, and 50 kN) are experimental common-load checkpoints rather than independently defined code-based service loads. Because the lowest measured ultimate load is 50 kN, that checkpoint corresponds to failure for the two horizontal-joint specimens and must not be labeled an ordinary service condition.

TABLE V. SECANT STIFFNESS K AT 15, 30 AND 50 KN IN KN/MM, AND RETENTION R RELATIVE TO RB AT THE SAME LOAD IN PERCENT. K = P/Δ; R = 100K/KRB. VALUES ARE CALCULATED FROM TABLE 4 WITHOUT INFERRING INTERMEDIATE MEASUREMENTS.

Specimen	K15	K30	K50	R15 (%)	R30 (%)	R50 (%)
RB	6.82	6.98	5.00	100.00	100.00	100.00
HWCJB	5.17	5.08	3.88	75.86	72.88	77.52
HFCJB	4.69	4.76	3.70	68.75	68.25	74.07
VMCJB	5.36	5.08	3.94	78.57	72.88	78.74
IMCJB	5.77	5.45	4.17	84.62	78.18	83.33
KMCJB	6.52	6.52	4.76	95.65	93.48	95.24

At 30 kN, KMCJB retained approximately 93.5% of the reference secant stiffness. Because the first visible cracking loads were 9–13 kN, the three tabulated deflection checkpoints (15, 30, and 50 kN) permit interval-average post-cracking slopes, but do not identify the initial uncracked slope. The 50 kN endpoint equals the observed ultimate load of HWCJB and HFCJB; those latter interval averages must therefore be interpreted with particular care.

3.4.1 Interval-Based Post-Cracking Stiffness and Relative Degradation

Using the recorded midspan deflections at 15, 30, and 50 kN, the mean incremental stiffness for the two post-cracking intervals was calculated as $K_{15–30} = 15/(\delta_{30} - \delta_{15})$ and $K_{30–50} = 20/(\delta_{50} - \delta_{30})$, respectively, in kN/mm. The relative reduction of interval-average stiffness was $D = [1 - (K_{30–50}/K_{15–30})] \times 100\%$. These are finite-interval secant slopes between measured points, not instantaneous tangent stiffness values. No intervening data were generated or interpolated.

TABLE VI. AVERAGE INCREMENTAL STIFFNESS IN THE OBSERVED POST-CRACKING LOAD INTERVALS, WITH RELATIVE REDUCTION BETWEEN INTERVALS. ALL STIFFNESS VALUES IN KN/MM.

Specimen	K15–30	K30–50	Reduction (%)
RB	7.14	3.51	50.9
HWCJB	5.00	2.86	42.9
HFCJB	4.84	2.78	42.6
VMCJB	4.84	2.94	39.2
IMCJB	5.17	3.08	40.5
KMCJB	6.52	3.39	48.0

Across the six specimens, the interval-average stiffness decreased between the 15–30 and 30–50 kN intervals by approximately 39.2–50.9%. RB showed 7.14 and 3.51 kN/mm, and KMCJB showed 6.52 and 3.39 kN/mm, respectively. The lower percentage decrease of some jointed beams does not indicate greater absolute stiffness or structural superiority. The first tabulated load (15 kN) exceeds the measured first-visible-crack loads of all specimens (9–13 kN); consequently, initial pre-cracking stiffness cannot be determined reliably from this table. These differences are descriptive, because no structural replicate tests were available.

3.5 Scope, Statistical Interpretation, and Related Experimental Programme

One structural specimen was tested per configuration, including one monolithic control. The results are exploratory, specimen-specific comparisons rather than statistically significant differences or evidence of equivalence. A separate manuscript under review examines three shear-span joint configurations from the same casting programme and shares the monolithic reference specimen and concrete material tests. Its jointed specimens differ from the three midspan and two horizontal-joint specimens examined here. The shared reference is not an additional replicate. Identifying details of the related submission are disclosed confidentially to the Editor-in-Chief. Fig. 7 summarizes the recorded first-visible-crack and ultimate loads for these six distinct specimens.

The material-cube sample standard deviations quantify variation among the three cubes from each placement and must not be interpreted as replicate T-beam results. Local slip, crack width, reinforcement yield strain, initial tangent stiffness, post-cracking tangent stiffness and instrument calibration uncertainty were not measured or cannot be recovered from the currently available data. The 50 kN comparison is at the observed failure load of the two horizontal-joint beams, and consequently should not be characterized as strictly pre-failure for every specimen.

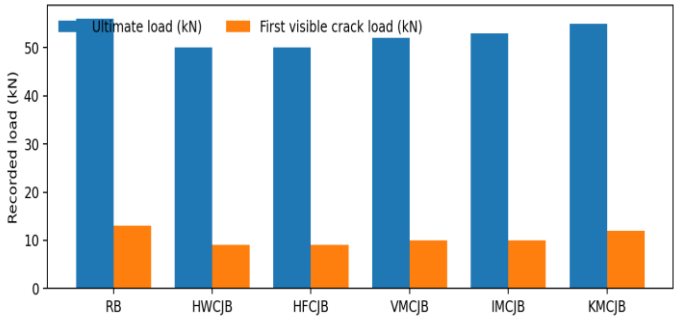


Fig. 7. Descriptive comparison of recorded first-visible-crack and ultimate loads for the six distinct structural specimens (one test per configuration).

3.6 Interpretation of Force Transfer at Construction Joints

Mechanisms potentially relevant to staged concrete include interface adhesion prior to debonding, friction under normal compression, aggregate interlock across rough surfaces, and dowel and clamping action from reinforcing bars that actually intersect the interface. The nonplanar keyed detail may additionally develop bearing and geometrical interlock. These contributions are coupled and depend on local stress and displacement; the current tests measured overall member response rather than their individual shares. The near-reference capacity of the keyed specimen (55 versus 56 kN) is therefore consistent with, but does not prove, a dominant mechanical-interlock mechanism. Absence of visually evident separation in photographs is not proof of zero slip; yielding of tension reinforcement was also not directly verified. Reinforcement crossing an interface may contribute dowel and clamping actions [6,9]. Beam failure load cannot uniquely identify independent interface shear capacity.

3.7 Relation to Published Experimental Work

Jabir et al. [12] tested seven 200 × 100 × 1000 mm reinforced-concrete beams under monotonic central loading. They reported strength reductions of 5–7.5% for tension-zone horizontal joints and 1.25–2.5% for inclined joints. The present T-beams showed 10.7% and 5.4% reductions, respectively. These are study-specific changes rather than a common effect size because section shape, joint location, reinforcement and geometry differ. Aziz and Ajeel [7] reported approximately 27% lower shear capacity for T-beams with flange cold joints, a different endpoint from the present flexure-dominated ultimate-load comparison. Issa et al. [8] reported 24–83% reductions in plain-concrete modulus of rupture, which cannot be interpreted as reinforced-beam ultimate-load reductions. Jang et al. [10] used push-off tests with UHPC and normal-strength-concrete interfaces and different surface treatments, measuring local shear rather than beam flexural response. These differences prevent universal ranking across studies.

3.8 Practical Implications and Limitations

Data provenance and related submission. The monolithic reference specimen and concrete material tests are shared with a companion manuscript on shear-span construction joints under review at another journal. The present analysis concerns midspan and horizontal construction joints. The common reference is identified explicitly to avoid treating reused measurements as independent replication.

Construction-joint location and detailing must be assessed against member bending and shear demand, reinforcement continuity, interface preparation, construction sequence and applicable design-code requirements. The small measured reduction for the keyed detail does not justify treating it as equivalent to monolithic construction in full-scale design. The study includes one specimen per configuration, one concrete mixture and reinforcement arrangement, one nominal beam size, and monotonic three-point bending only. It does not establish cyclic/fatigue response, crack-width evolution, local interfacial transfer, steel yielding or full-scale design provisions. Replicate tests and local interface instrumentation are necessary to examine reproducibility and possible mechanisms before general recommendations can be made. A nonlinear interface-contact model was not developed or validated; future modelling requires independent calibration and experimental validation.

Under a central point load P on a simply supported effective span L = 1.00 m, the nominal peak moment is PL/4 and each shear-span force is P/2. At the six recorded ultimate loads, these relations describe global sectional actions only; they do not independently measure construction-joint interface shear capacity.

4. CONCLUSIONS

Within the scope of the six tested reinforced-concrete T-beams, the following conclusions are supported directly by the experimental results:

1. The observed cracking and failure appearances were consistent with flexure-dominated behavior, but steel yielding was not independently verified by reinforcement strain measurements. No obvious macroscopic joint separation was reported, and local interface slip was not measured.

2. The first visible crack load was most strongly affected by the horizontal joints. HWCJB and HFCJB showed a 30.8% reduction relative to RB, whereas the reductions were 23.1% for VMCJB and IMCJB and 7.7% for KMCJB (computed from the displayed whole-kN load measurements).

3. Relative to the 56 kN reference, ultimate loads were 50 kN for both horizontal-joint specimens, 52 kN for VMCJB, 53 kN for IMCJB and 55 kN for KMCJB. Reductions were 10.7%, 7.1%, 5.4% and 1.8%, respectively. These single-specimen differences do not establish statistical equivalence or causal separation from specimen variability.

4. Construction joints increased mid-span deflection at all three comparison load levels. At 50 kN, the increases relative to RB were 29% for HWCJB, 35% for HFCJB, 27% for VMCJB, 20% for IMCJB, and 5% for KMCJB.

5. Among the tested midspan configurations, KMCJB had the closest measured first-visible-crack load, ultimate load and common-load deflection to RB. IMCJB had a higher ultimate load and lower common-load deflections than VMCJB. These comparisons apply to the individual specimens and do not establish the separate contribution of mechanical interlock.

6. These conclusions are confined to measured global responses and qualitative failure observations for the six tested beams, with the stated geometry, material information, reinforcement, joint details and monotonic loading. One specimen per configuration, limited material-record traceability and absent local interface/strain measurements prevent general design rules, statistical inference or quantitative attribution of transfer mechanisms.

CRediT Author Contributions

Falah J. Alkhafaji: Conceptualization, Methodology, Investigation, Formal analysis, Writing – original draft, Writing – review & editing.

Mohammed A. Jennam: Methodology, Investigation, Data curation, Resources, Writing – review & editing.

Ashraf Hameed Alsalmani: Conceptualization, Formal analysis, Visualization, Validation, Writing – original draft, Writing – review & editing, Project administration.

Amer F. Izzet: Methodology, Validation, Supervision, Resources, Writing – review & editing.

All authors have read and approved the final version of the manuscript and agreed to be accountable for their respective contributions.

Conflicts of Interest

The authors declare that they have no conflicts of interest related to this research.

Funding

This research received no external funding.

Acknowledgments

The authors have no additional acknowledgments to declare.

Ethical Approval

Ethical approval was not required, as this study involved only laboratory experiments on reinforced-concrete beam specimens.

Data Availability Statement

The experimental data supporting the findings of this study are available from the corresponding author upon reasonable request.

Declaration of Generative AI and AI-Assisted Technologies in the Writing Process

During the preparation of this manuscript, the authors used ChatGPT to improve language, academic phrasing, and readability. The authors reviewed and edited the content and take full responsibility for the final manuscript.

References

[1] S. I. Ammar and A. S. Mahmoud, “State of art of construction joints of reinforced concrete beams,” in Proceedings of the 2nd International Conference of Engineering Science (CESC), 2024, doi: 10.31272/conf.CESC.7.

[2] Z. W. Abass, “Effect of construction joints on performance of reinforced concrete beams,” Al-Khwarizmi Engineering Journal, vol. 8, no. 1, pp. 48–64, 2012.

[3] R. J. Aziz, “Shear capacity of concrete prisms with interface joints,” Journal of Engineering, vol. 16, no. 2, pp. 5084–5097, 2010, doi: 10.31026/j.eng.2010.02.24.

[4] Q. Abdul-Majeed, L. A. Ghaleb, and M. G. Ghaddar, “Effect of the number of horizontal construction joints in reinforced concrete beams,” Engineering and Technology Journal, vol. 28, no. 19, pp. 5803–5821, 2010, doi: 10.30684/etj.28.19.1.

[5] A. H. Aziz, “Flexural and shear behavior of hybrid I-beams with high-strength concrete and steel fibers,” Ph.D. dissertation, Department of Civil Engineering, Al-Mustansiriyah University, 2006.

[6] ACI Committee 224, Joints in Concrete Construction, ACI 224.3R-95, American Concrete Institute, Farmington Hills, MI, USA, 1995 (reapproved 2013).

[7] A. H. Aziz and A. E. Ajeel, “Effect of existing flange opening and cold joints on strength of RC T-beams,” Journal of Engineering, vol. 16, no. 1, pp. 4535–4546, 2010, doi: 10.31026/j.eng.2010.01.11.

[8] C. A. Issa, N. N. Gerges, and S. Fawaz, “The effect of concrete vertical construction joints on the modulus of rupture,” Case Studies in Construction Materials, vol. 1, pp. 25–32, 2014, doi: 10.1016/j.cscm.2013.12.001.

[9] N. N. Gerges, C. A. Issa, and S. Fawaz, “The effect of construction joints on the flexural bending capacity of singly reinforced beams,” Case Studies in Construction Materials, vol. 5, pp. 112–123, 2016, doi: 10.1016/j.cscm.2016.09.004.

[10] H. O. Jang, H. S. Lee, K. Cho, and J. Kim, “Experimental study on shear performance of plain construction joints integrated with ultra-high-performance concrete (UHPC),” Construction and Building Materials, vol. 152, pp. 16–23, 2017, doi: 10.1016/j.conbuildmat.2017.06.156.

[11] M. H. Bin Osman, H. B. Tami, and N. A. Abdul Rahman, “A comparison of construction joint ability on concrete slab applied at construction site,” ARPN Journal of Engineering and Applied Sciences, vol. 11, no. 4, pp. 2576–2580, 2016.

[12] H. A. Jabir, T. S. Salman, and J. M. Mhalhal, “Effect of construction joints on the behavior of reinforced concrete beams,” Journal of Engineering, vol. 23, no. 5, pp. 47–60, 2017, doi: 10.31026/j.eng.2017.05.04.

[13] ASTM International, Standard Specification for Deformed and Plain Carbon-Steel Bars for Concrete Reinforcement, ASTM A615/A615M, West Conshohocken, PA, USA, 2016.

[14] ASTM International, Standard Specification for Steel Wire, Deformed, for Concrete Reinforcement, ASTM A496/A496M-07, West Conshohocken, PA, USA, 2007 (withdrawn 2013).

[15] J. M. Gere and S. P. Timoshenko, Mechanics of Materials, 4th ed. Boston, MA, USA: PWS Publishing Company, 1997.